ACS OMEGA

http://pubs.acs.org/journal/acsodf

Article

Pd-Decorated WTe_2 Monolayer as a Favorable Sensing Material toward SF_6 Decomposed Species: A DFT Study

Zhuoli Xu, Hao Cui, and Guozhi Zhang*

Cite This: *ACS Omega* 2023, 8, 4244−4250

Read Online

ACCESS | Metrics & More | Article Recommendations

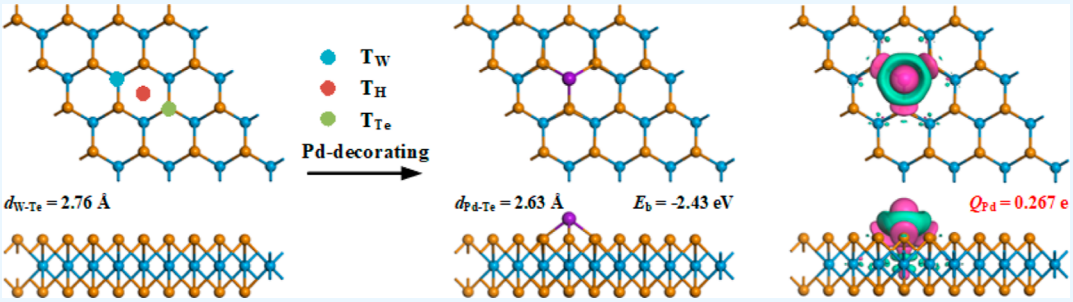

ABSTRACT: Based on density functional theory, this work first investigates the Pd-decorating property on the pristine WTe_2 monolayer and then simulates the adsorption performance of a Pd-decorated WTe_2 (Pd−WTe_2) monolayer on SO_2 and SOF_2 molecules, in order to explore its sensing potential for SF_6 decomposed species. It is found that the Pd atom can be stably anchored on the top of the W atom of the WTe_2 monolayer with a binding energy of −2.43 eV. The Pd−WTe_2 monolayer performs chemisorption on SO_2 and SOF_2, with adsorption energies of −1.36 and −1.17 eV, respectively. The analyses of the band structure and density of states reveal the deformed electronic property of the WTe_2 monolayer by Pd-decoration, as well as that of the Pd−WTe_2 monolayer by gas adsorption. The bandgap of the Pd−Wte_2 monolayer is increased by 1.6% in the SO_2 system and is decreased by −3.9% in the SOF_2 system, accounting for the sensing response of 42.0 and −56.7% for the detection of two gases. Moreover, the changed work function (WF) in two gas systems in comparison with that of the pristine Pd−WTe_2 monolayer suggests its potential as a WF-based gas sensor for sensing two gases as well. This paper uncovers the gas sensing potential of the Pd−WTe_2 monolayer to evaluate the operation status of SF_6 insulation devices, which also illustrates the strong potential of WTe_2-based materials for gas sensing applications in some other fields.

1. INTRODUCTION

SF_6, as a high-performance insulation medium, is widely applied in electrical engineering; it is injected into the high-voltage equipment to prevent the insulation defects such as partial discharge and partial overheat[1] and plays a significant role in guaranteeing the insulation performance of the whole power system. However, after several decades of running of SF_6 insulation devices, the SF_6 gas would be decomposed by the released energy of the insulation defects into unstable SF_x (x = 1−5), and SF_x would interact with trace water and oxygen, forming many stable gaseous compounds.[2] It has been reported that the early formed stable gas species is SOF_2, followed by SO_2 and some other species such as SO_2F_2 and CF_4.[3−5] The issue is that the newly formed gases exhibit a quite low insulation performance and would impair the insulation behavior of high-voltage devices.[6,7] Therefore, the early detection of these gas species can realize two purposes: (i) evaluate the discharge or overheat severity of SF_6 gas and (ii) guarantee the good operation of the SF_6 insulation devices.[8−10] Such a technique is nowadays widely accepted as a critical and workable manner to diagnose the potential defects in the operated power system.

In recent years, nanomaterial-based gas sensors develop significantly and have been regarded as an effective technique for gas detection, especially in some harsh environments for their merits of desirable sensitivity and rapid response.[11−14] Very recently, 2D transition-metal dichalcogenides (TMDs) have been tremendously studied for gas detection through experimental and theoretical techniques,[15−17] and some of them are reported with good sensing performance to SF_6 decomposed species.[18] These demonstrate the strong potential for exploration of 2D TMDs as novel gas sensing materials to detect decomposed species of SF_6 in the insulated devices.[19,20]

Received: November 21, 2022
Accepted: December 30, 2022
Published: January 19, 2023

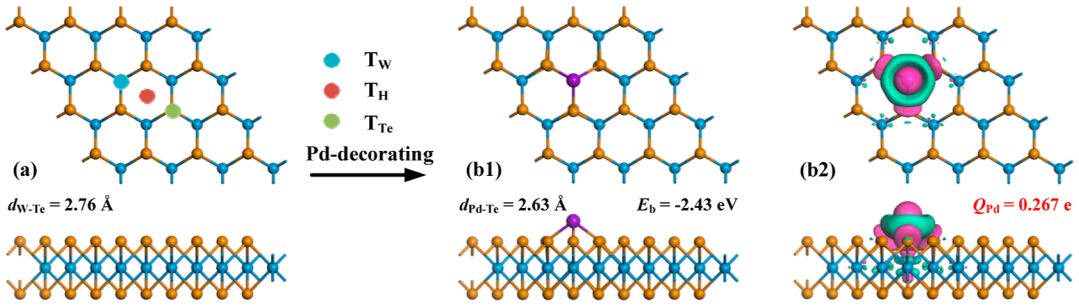

Figure 1. Pd-decorating process on the WTe_2 monolayer. (a) Pristine WTe_2 monolayer. (b1,b2) Preferred configuration and CDD of Pd−WTe_2 monolayer. In CDD, the cyan areas indicate electron accumulation and the violet areas denote electron deletion, with the isosurface of 0.01 eV/Å^3.

Considering the favorable gas sensing property of MoX_2 (X = S, Se, and Te),[21−24] scholars continue to explore the sensing performance of WS_2 and WSe_2 for detection of decomposed species of SF_6 from a theoretical perspective.[25−27] It should be noted that WX_2 are also proven to have a unique structure and admirable sensing property in comparison with MoX_2,[28,29] therefore, until now, little has been reported about WTe_2 sensing decomposed species of SF_6. Besides, there have been many reports highlighting the metal-doped WX_2 for gas sensing applications, since it can obviously promote the carrier mobility and chemical reactivity of WX_2, thus enhancing their sensing performance.[30,31] In this regard, we think that the metal-doped WTe_2 should be explored to uncover its potential as a gas sensor and to fill in such a gap.

In this work, we use density functional theory (DFT) to investigate the adsorption and sensing potentials of a Pd-decorated WTe_2 (Pd−WTe_2) monolayer upon SO_2 and SOF_2, in order to realize the operation mechanism of SF_6 insulation devices. The Pd atom is selected due to its strong and admirable catalytic property in the gas adsorption and sensing systems;[32−34] therefore, we assume that Pd decoration can show a favorable sensing response to the gas species. The findings of this work indicate the strong potential of the Pd−WTe_2 monolayer as a gas sensor for SO_2 and SOF_2 detection and also uncovers the tunable electronic property of the WTe_2 monolayer, which indicates its strong potential for exploration in some other fields.

2. COMPUTATIONAL DETAILS

The DFT calculations in this work were conducted in the DMol^3 package,[35] including the Pd-decorating process on the WTe_2 monolayer and the gas adsorption processes, in which the Perdew−Burke−Ernzerhof function within the generalized gradient approximation was defined to consider the exchange correlation interactions,[36] and the DFT-D2 method was employed to deal with the van der Waals force and long-range interactions.[37] The *k*-point mesh of 10 × 10 × 1 was adopted in the Brillouin zone integration,[38] and the energy tolerance accuracy, maximum force, and displacement were defined to be 10^{-5} Ha, 2 × 10^{-3} Ha/Å, and 5 × 10^{-3} Å,[22] respectively. Also, the self-consistent loop energy of 10^{-6} Ha and the global orbital cut-off radius of 5.0 Å were applied to ensure the accuracy of the total energy.[39]

A 4 × 4 × 1 supercell was established for the WTe_2 monolayer, which contains 16 W atoms and 32 Te atoms with a vacuum region of 15 Å along the *z* direction to prevent the possible interactions between the adjacent units.[40] The binding energy (E_b) was determined to reflect the binding force between the Pd dopant and the WTe_2 monolayer, calculated as[41]

$$E_b = E_{Pd-WTe_2} - E_{WTe_2} - E_{Pd} \quad (1)$$

where E_{Pd-WTe_2} and E_{WTe_2} mean the total energy of the Pd-decorated and intrinsic WTe_2 monolayers, respectively, and E_{Pd} is the energy of the single Pd atom in its bulk structure.[42] At the same time, the adsorption energy (E_{ad}) was calculated to evaluate the binding strength between the Pd−WTe_2 monolayer and the gas species and is expressed as[43]

$$E_{ad} = E_{Pd-WTe_2/gas} - E_{Pd-WTe_2} - E_{gas} \quad (2)$$

where $E_{Pd-WTe_2/gas}$, E_{Pd-WTe_2}, and E_{gas} are the energies of the Pd−WTe_2/gas system, the isolated Pd−WTe_2 system, and the gas molecule, respectively. We applied the Hirshfeld method to consider the charge transfer (Q_T) of the gas species in adsorption, the positive value of which indicates the electron-donating property of the adsorbed molecule.

3. RESULTS AND DISCUSSION

3.1. Pd-Decorating Property of the WTe_2 Monolayer.

We first establish and optimize the geometric structure of the pristine WTe_2 monolayer and then conduct the Pd-decorating process on its surface, for which we consider three possible sites, termed T_W (at the top of the W atom), T_H (at the top of the hollow site), and T_{Te} (at the top of the Te atom). The process is displayed in Figure 1, in which the charge density difference (CDD) of the preferred Pd−WTe_2 monolayer is shown as well for a better understanding of the charge-transfer behavior in this process.

For the pristine WTe_2 monolayer, the W−Te bond is measured as 2.76 Å and the constant lattice is obtained as 3.55 Å, which are in good accordance with the previous report in ref.[44] For the Pd−WTe_2 monolayer, one can see that the preferred configuration for Pd-decoration on the WTe_2 monolayer is through the T_W site with an E_b of −2.43 eV. It should be mentioned that the E_b for Pd-decoration on the T_H and T_{Te} sites is calculated as −1.76 and −2.38 eV, respectively. These findings reveal the strongest interaction between the Pd atom and the WTe_2 monolayer at the T_W site and the best stability of the determined Pd−WTe_2 configuration. Such findings are consistent with the Ni-decoration on the WTe_2 monolayer.[44] Besides, vibrational analysis shows that the frequencies of the Pd−WTe_2 monolayer range from 44.41 to 246.03 cm^{-1}, without an imaginary frequency, indicating the stably-anchored Pd atom on the WTe_2 surface,[45] namely, good thermostability. The Pd−Te bond lengths are obtained as 2.63 Å, which is slightly shorter than the covalent radii of Pd and Te

https://doi.org/10.1021/acsomega.2c07456
ACS Omega 2023, 8, 4244−4250

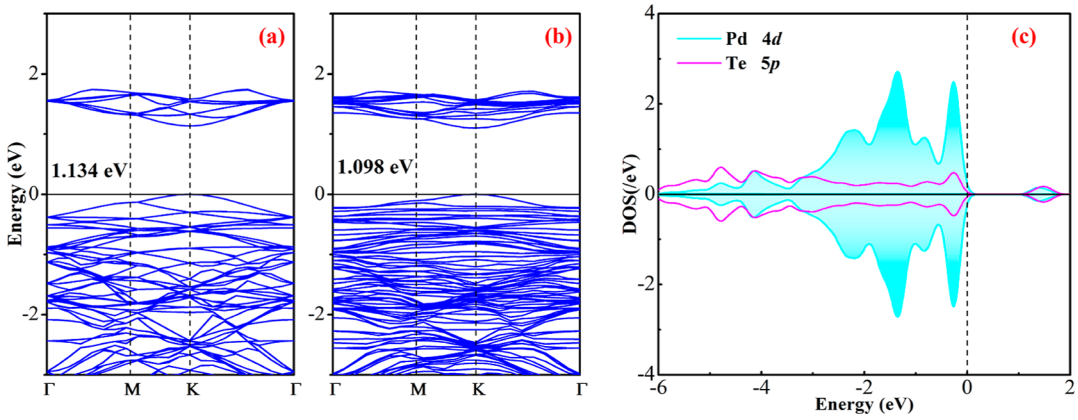

Figure 2. BS (a,b) and DOS (c) of the Cu-doping property on the $MoTe_2$ monolayer. The black values are bandgaps in the BS and the dashed line in the DOS means the Fermi level.

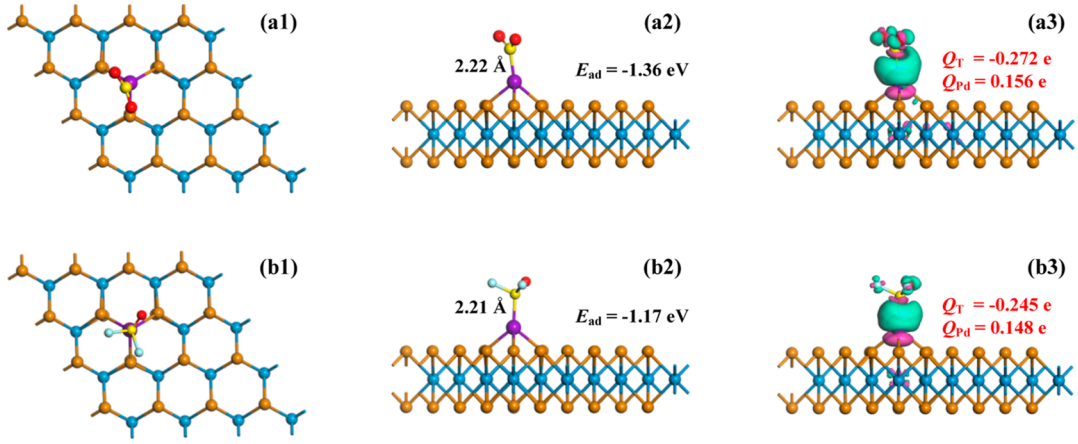

Figure 3. MSC in top and side views and CDD in side view of (a) the SO_2 system and (b) the SOF_2 system. The black values are atomic distances, and the set in CDD is the same as Figure 1.

atoms (2.57 Å[46]), suggesting the stronger ionic bond nature in comparison with the covalent bond nature in the formation of Pd−Te bonds.[47]

From Hirshfeld analysis, the Pd adatom is positively charged by 0.267*e*, while the bonded three Te atoms are charged equally by −0.024*e*, respectively. Compared with the charged value of equally 0.013*e* for the Te atom in the pristine WTe_2 monolayer, one can see that the Te atoms in the Pd-decorating process exhibit strong electron-accepting property, withdrawing 0.111*e* in total for all three Te atoms. That is, the WTe_2 monolayer as a whole accepts 0.267*e* from the Pd adatom, in which three Te atoms accept 0.111*e*, revealing the desirable electronegativity of the W and Te atoms in this system.[48] Also, the positively charged Pd atom and the negatively charged Te atom reveal the ionic bond nature of the new-formed Pd−Te bonds where the electrostatic attraction occurs. According to the CDD, the Pd dopant is surrounded by electron depletion, while the Pd−Te bonds are surrounded by electron accumulation, which confirms the electron-donating property of the Pd adatom and the strong orbital interactions in the Pd−Te bonds to accelerate their formation.

The band structure (BS) of the pristine and Pd-decorated WTe_2 monolayer as well as the orbital density of state (DOS) of the bonded atoms are depicted in Figure 2 to help comprehend the electronic property of the WTe_2 monolayer during Pd-decoration. From the BS of the pristine WTe_2 monolayer, it is seen that the maximum valence band and the minimum conduction band are both located at the *K* point with the bandgap of 1.134 eV. These results indicate the direct semiconducting property for the pristine WTe_2 monolayer, in agreement with ref.[44] For the Pd−WTe_2 monolayer, it is found that the maximum valence band and the minimum conduction band are both located at the *K* point as well, indicating that Pd-decoration has little impact on the direct semiconducting property of the WTe_2 monolayer. Besides, the bandgap of the Pd−WTe_2 monolayer is obtained as 1.098 eV, reducing by 0.036 eV (3.17%) in comparison to the pristine WTe_2 system. Also, one can see that the electronic states are much denser in the Pd−WTe_2 system than the pristine WTe_2 system, which indicates that Pd-decoration induces a lot of novel states in the electronic states of the WTe_2 system and that some even fill in its bandgap, thereby giving rise to the narrowed bandgap for the Pd−WTe_2 monolayer. From the atomic DOS, one can see that the Pd 4d orbital is highly overlapped with the Te 5p orbital at −6−0 and 1.4 eV, which proves the strong orbital interactions between the Pd and Te atoms, confirming the electron hybridization of Pd−Te bonds in the CDD and verifying the strong binding force for Pd-decoration on the WTe_2 surface. Moreover, the top valence band and the bottom conduction band are, respectively, located on the Pd and Te atoms, which suggests the charge transfer from Pd to the Te atoms, verifying the Hirshfeld analysis.[49]

3.2. Gas Adsorption on the Pd−WTe_2 Monolayer. At the top of the Pd−WTe_2 monolayer, adsorption of SO_2 and

https://doi.org/10.1021/acsomega.2c07456
ACS Omega 2023, 8, 4244−4250

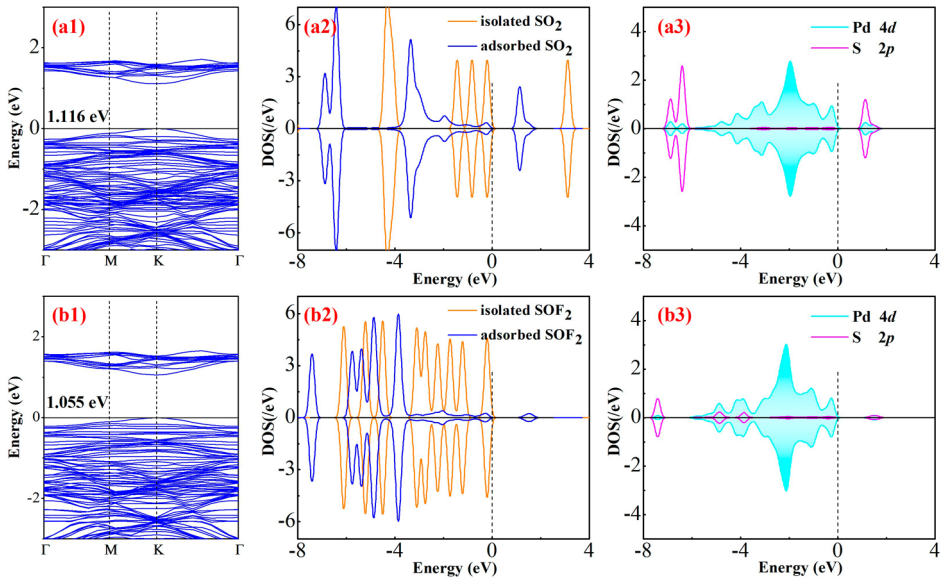

Figure 4. BS, molecular DOS and orbital DOS of gas adsorbed systems. (a1−a3) SO_2 system and (b1−b3) SOF_2 system. In BS, the black values are bandgaps, while the dashed line in the DOS is the Fermi level.

SOF_2 is performed, and the gas adsorption systems are established by putting the gas species around the Pd adatom via various configurations with the atomic distance of approximately 2.5 Å. After geometric optimization, we can obtain several E_{ad} for each adsorption system using eq 2, and we define the configuration with the most negative E_{ad} as the most stable configuration (MSC) for further analysis. For SO_2 and SOF_2 adsorption systems, the MSC and CDD are exhibited in Figure 3.

In the SO_2 adsorption system, one can see that the SO_2 molecule is basically vertical to the WTe_2 surface, with the S atom trapped by the Pd adatom and two S−O bonds pointing to the vacuum region. The Pd−S bond is measured as 2.22 Å, which is slightly shorter than the summed covalent radii of Pd and S atoms (2.23 Å[46]), indicating the strong covalent bond nature and binding force in the formed Pd−S bond. The Pd−Te bonds are increased to 2.68, 2.70, and 2.72 Å, respectively, from the equal bond lengths of 2.63 Å in the isolated Pd−WTe_2 system, which indicates its slightly deformed morphology caused by SO_2 adsorption. The E_{ad} in this system is calculated to be −1.36 eV, which is more negative than the critical value of −0.8 eV for the identification of chemisorption.[50] That is, we assume the adsorption of the SO_2 molecule on the Pd−WTe_2 monolayer as strong chemisorption. From Hirshfeld analysis, we find that the adsorbed SO_2 molecule is charged by −0.272*e*, implying its electron-accepting property. Given the positive charge value of 0.156*e* for the Pd adatom, we can infer that the WTe_2 surface loses 0.383*e* in SO_2 adsorption, in which the Pd atom accepts 0.111*e* and the Pd atom accepts 0.272*e*. From CDD, we infer that there is strong electron accumulation on the Pd−S bonds and the Pd adatom, which not only reveals the favorable orbital interaction in the formation of Pd−S bonds but also verify the electron-accepting property of the Pd atom.[51] Also, there has been somewhat electron depletion on the Pd−Te bonds, which suggest the slightly weakened binding force on the Pd−Te bonds, in accordance with their increase after SO_2 adsorption.[52]

Upon SOF_2 adsorption on the Pd−WTe_2 monolayer, it is seen that the SOF_2 molecule prefers to be trapped by the Pd adatom in the S-end position, and the S−O and two S−F bonds point to the vacuum region. The formed Pd−S bond is measured to be 2.21 Å; therefore, the strong covalent bond nature can also be determined, giving rise to the admirable binding force of the formed Pd−S bond. The Pd−Te bonds also undergo some increase to 2.68, 2.69, and 2.69 Å, respectively, which is not as high as that in the SO_2 system, implying the relatively weaker interaction in the SOF_2 system. In fact, the E_{ad} herein is calculated as −1.17 eV, not as negative as that in the SO_2 adsorption system, verifying the weaker interaction here. However, such a value can identify the SOF_2 adsorption as chemisorption as well. According to the CDD distribution, the Pd−S bond is surrounded with electron accumulations, confirming the strong electron hybridization and orbital interaction here, while the embraced electron depletion on the Pd−Te bonds verifies their weakness after SOF_2 adsorption. Based on Hirshfeld analysis, the SOF_2 molecule is negatively charged, 0.245*e*, while the Pd adatom is positively charged, 0.148*e*. These findings reveal that the WTe_2 surface loses 0.364*e* in the SOF_2 adsorption, in which the Pd adatom accepts 0.119*e*, while the SOF_2 molecule accepts 0.245*e*.

In short, the Pd−WTe_2 monolayer has strong chemisorption in the SO_2 and SOF_2 systems, in which the SO_2 and SOF_2 molecules both exhibit strong electron-accepting property. Besides, the Pd adatom behaves as an electron bridge, accelerating the charge transfer from the WTe_2 surface to the gas species, and the Pd adatom also accepts electrons during gas interactions. The electron accumulation distributions confirm the formation of new bonds, and the electron depletion verifies the deformation in the Pd−WTe_2 monolayer during gas adsorption.

3.3. Electronic Properties of the Pd−WTe_2/Gas Systems. The charge transfer in the gas adsorption can modulate the electronic property of the Pd−WTe_2 monolayer, which can also provide the sensing mechanism for gas detection. Therefore, we plot the BS of the gas adsorbed systems, the molecular DOS of the adsorbed gases, and the orbital DOS of the bonded atoms to illustrate the electronic

https://doi.org/10.1021/acsomega.2c07456
ACS Omega 2023, 8, 4244−4250

property of the Pd−WTe_2 monolayer in SO_2 and SOF_2 adsorptions, as seen in Figure 4.

From the BS distributions, it is found that the maximum valence band and the minimum conduction band for two gas systems are both located at the *K* point, indicating the non-impacted direct semiconducting property of the Pd−WTe_2 monolayer in the gas adsorption. On the other hand, the bandgap of the Pd−WTe_2 monolayer is increased to 1.116 eV, by 1.6%, in the SO_2 system, while it is decreased to 1.055 eV, by −3.9%, in the SOF_2 system. Such changes can be attributed to the gas adsorptions, in which the activated electronic states of the adsorbed gases contribute largely to the whole adsorbed system. The activation of the electronic states in the gas species can be found in the molecular DOS. One can see that the states of the isolated SO_2 and SOF_2 molecules are split into several small states and are left-shifted to different degrees. Besides, it is the activated electronic states of the gas species undergoing strong hybridization with the Pd dopant that facilitate the formation of new bonds in the gas adsorbed systems. Specifically, the Pd 4d orbital is highly overlapped with the S 2p of the SO_2 molecule at −6.9, −6.1, and 1.2 eV and is highly overlapped with the S 2p of the SOF_2 molecule at −7.4, −5.9, and −3.9 eV, respectively. These state hybridizations manifest the strong orbital interaction between the atoms and verify the formation of new bonds. Moreover, it is worth noting that the top of the valence band and the bottom of the conduction band are both located at the Pd adatom and the S atom of the gas species (SO_2 or SOF_2) in two gas adsorbed systems. These findings indicate the charge transfer from the Pd atom to the S atom (or gas species), which is consistent with Hirshfeld analysis and reveals the electron-accepting property of two gas species during their adsorption.

3.4. Gas Sensor Explorations. The electronic bandgap of the Pd−WTe_2 monolayer is afflicted with different degrees of change in two gas systems; therefore, we presume that the electrical conductivity of the Pd−WTe_2 monolayer would experience dramatic change as well, considering the dependence between the electrical conductivity (σ) and the bandgap (B_g) of the materials, expressed as

$$\sigma = e^{(-B_g/2kT)} \tag{3}$$

wherein *T* is the temperature and *k* is the Boltzmann constant (1.38×10^{-23} J/K). Besides, the changed electrical conductivity can provide the potential of the Pd−WTe_2 monolayer as a resistance-type gas sensor, in which the gas sensing response (S) can be calculated as[53]

$$S = (\sigma_{gas}{}^{-1} - \sigma_{pure}{}^{-1})/\sigma_{pure}{}^{-1} \tag{4}$$

in which σ_{gas} and σ_{pure} are the electrical conductivity of the Pd−WTe_2/gas system and the isolated Pd−WTe_2 monolayer, respectively.

Through calculations using eqs 3 and 4, the sensing response of the Pd−WTe_2 monolayer to SO_2 and SOF_2 at room temperature are 42.0 and −56.7%, respectively. These results reveal that the Pd−WTe_2 monolayer performs a positive sensing response upon SO_2 detection, while a negative sensing response to SOF_2 detection. For one thing, the sensing response in SO_2 and SOF_2 systems is large enough for detections using the electrochemical workstation;[54] for another, the opposite changing tendency of electrical conductivity in two systems gives the potential for selectivity detection of such two gases in their own surrounding. From these aspects, we consider that the Pd−WTe_2 monolayer is a promising candidate to be explored as a resistance-type gas sensor for SO_2 and SOF_2 detection with favorable sensitivity.[55]

Moreover, the recovery property of the Pd−WTe_2 monolayer can be analyzed from van't-Hoff−Arrhenius theory,[56] expressed as

$$\tau = A^{-1}e^{(-E_{ad}/kT)} \tag{5}$$

wherein *A* is the attempt frequency which we select in this work, 1×10^{16} Hz[57] (UV light), *k* is the Boltzmann constant, and *T* is the temperature. Based on eq 5, the required times for SO_2 or SOF_2 desorption from the Pd−WTe_2 surface at room temperature (298 K) are calculated to be 9.8×10^6 and 6015.5 s, respectively, and are obtained as 16.4 and 0.06 s, respectively, at 398 K. These findings manifest that the heating process at 398 K under UV light is necessary to realize the recycle use of the Pd−WTe_2 monolayer for gas detection, while at room temperature it is not realistic to desorb the adsorbed gas species.

The work function (WF) of the pristine and Pd-decorated WTe_2 monolayers as well as of the gas-adsorbed systems is analyzed to deeply elucidate the electron-overflow performance of various systems, with the WF values displayed in Figure 5, in which the WF values are the opposite number of the Fermi level. According to this figure, it is seen that the WF of the Pd−WTe_2 monolayer (4.45 eV) is slightly smaller than the pristine WTe_2 monolayer (4.47 eV), indicating that Pd-decoration can weaken the difficulty for the WTe_2 monolayer to realize an electron at the vacuum level.[58] Besides, the WFs of SO_2 and SOF_2 systems are increased to 4.66 and 4.62 eV, respectively. Such an obvious increase in the WF of the Pd−WTe_2 monolayer, by 4.3% for SO_2 adsorption and 3.4% for SOF_2 adsorption, proves its strong potential for SO_2 and SOF_2 detection using a Kelvin oscillator device.[59] In other words, the Pd−WTe_2 monolayer can be explored as a WF-based gas sensor for sensing SO_2 and SOF_2 as well. However, the selective detection of SO_2 and SOF_2 cannot be fulfilled using a WF-based gas sensor considering the tiny difference in WF between the two systems.

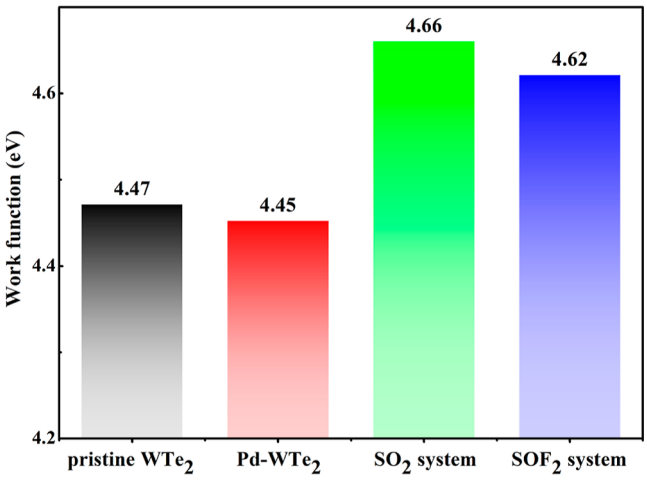

Figure 5. WF of pristine and Pd-decorated WTe_2 monolayer as well as of gas systems.

https://doi.org/10.1021/acsomega.2c07456
ACS Omega 2023, 8, 4244−4250

4. CONCLUSIONS

This work based on DFT proposes the Pd−WTe_2 monolayer as a novel sensing material for detection of SO_2 and SOF_2 in SF_6 insulation devices, and there are four significant findings that should be highlighted, which are listed as follows:

(i) The Pd atom is stably anchored on the T_W site of the WTe_2 monolayer, with the E_b of −2.43 eV, narrowing the bandgap to 1.098 eV for the Pd−WTe_2 monolayer;
(ii) Chemisorption is identified for SO_2 and SOF_2 adsorption on the Pd−WTe_2 monolayer, with E_{ad} of −1.36 and −1.17 eV, respectively;
(iii) The sensing response of the Pd−WTe_2 monolayer is 42.0% for the SO_2 system and −56.7% for the SOF_2 system, indicating its strong potential as a resistance-type gas sensor for selective detection of such two gases;
(iv) The changed WF in two gas systems in comparison with the pristine Pd−WTe_2 monolayer suggests its potential as a WF-based gas sensor for sensing two gases as well.

These findings manifest the great feasibility of the Pd−WTe_2 monolayer as a chemical gas sensor for SO_2 and SOF_2 detection in SF_6 insulation devices. Moreover, the tunable electronic property of the pristine WTe_2 monolayer indicates its potential for exploration in some other fields, such as gas catalysis and storage.

AUTHOR INFORMATION

Corresponding Author

Guozhi Zhang − *Hubei Engineering Research Center for Safety Monitoring of New Energy and Power Grid Equipment, Hubei University of Technology, Wuhan 430068, China;* orcid.org/0000-0002-0425-3836; Email: youzgz@163.com

Authors

Zhuoli Xu − *Hubei Engineering Research Center for Safety Monitoring of New Energy and Power Grid Equipment, Hubei University of Technology, Wuhan 430068, China*

Hao Cui − *College of Artificial Intelligence, Southwest University, Chongqing 400715, China;* orcid.org/0000-0002-9410-6345

Complete contact information is available at: https://pubs.acs.org/10.1021/acsomega.2c07456

Notes

The authors declare no competing financial interest.

ACKNOWLEDGMENTS

This work was supported by the National Natural Science Foundation of China (no. 52207175).

REFERENCES

(1) Cui, H.; Yan, C.; Jia, P.; Cao, W. Adsorption and sensing behaviors of SF6 decomposed species on Ni-doped C3N monolayer: A first-principles study. *Appl. Surf. Sci.* **2020**, *512*, 145759.
(2) Zhang, X.; Yu, L.; Gui, Y.; Hu, W. First-principles study of SF6 decomposed gas adsorbed on Au-decorated graphene. *Appl. Surf. Sci.* **2016**, *367*, 259−269.
(3) Zhang, X.; Gui, Y.; Xiao, H.; Zhang, Y. Analysis of adsorption properties of typical partial discharge gases on Ni-SWCNTs using density functional theory. *Appl. Surf. Sci.* **2016**, *379*, 47−54.
(4) Cui, H.; Liu, T.; Zhang, Y.; Zhang, X. Ru-InN Monolayer as a Gas Scavenger to Guard the Operation Status of SF6 Insulation Devices: A First-Principles Theory. *IEEE Sens. J.* **2019**, *19*, 5249−5255.
(5) Zeng, F.; Tang, J.; Xie, Y.; Zhou, Q.; Zhang, C. Experimence Study of Trace Water and Oxygen Impact on SF6 Decomposition Characteristics Under Partial Discharge. *J. Electr. Eng. Technol.* **2015**, *10*, 1786−1795.
(6) Wang, D.; Lan, T.; Pan, J.; Liu, Z.; Yang, A.; Yang, M.; Chu, J.; Yuan, H.; Wang, X.; Li, Y. J. S.; Rong, A. A. Janus MoSSe monolayer: A highly strain-sensitive gas sensing material to detect SF6 decompositions. *Sens. Actuators, A* **2020**, *311*, 112049.
(7) Liu, M.; Tang, J.; Liu, X.; Yao, Q.; Miao, Y. Study on the Characteristic Decomposition Components of DC SF6-Insulated Equipment under Positive DC Partial Discharge. *Energies* **2017**, *10*, 640.
(8) Cui, H.; Zhang, X.; Zhang, J.; Zhang, Y. Nanomaterials-based gas sensors of SF6 decomposed species for evaluating the operation status of high-voltage insulation devices. *High Voltage* **2019**, *4*, 242−258.
(9) Zhang, X.; Yu, L.; Tie, T.; Dong, X. Gas Sensitivity and Sensing Mechanism Studies on Au-Doped TiO2 Nanotube Arrays for Detecting SF6 Decomposed Components. *Sensors* **2014**, *14*, 19517−19532.
(10) Tang, J.; Liu, F.; Meng, Q.; Zhang, X.; Tao, J. Partial discharge recognition through an analysis of SF6 decomposition products part 2: feature extraction and decision tree-based pattern recognition. *IEEE Trans. Dielectr. Electr. Insul.* **2012**, *19*, 37−44.
(11) Cui, H.; Zhang, G.; Zhang, X.; Tang, J. Rh-doped MoSe2 as a toxic gas scavenger: a first-principles study. *Nanoscale Adv.* **2019**, *1*, 772−780.
(12) Cui, H.; Jia, P.; Peng, X. Adsorption of SO2 and NO2 molecule on intrinsic and Pd-doped HfSe2 monolayer: A first-principles study. *Appl. Surf. Sci.* **2020**, *513*, 145863.
(13) Yang, A.; Chu, J.; Li, W.; Wang, D.; Yang, X.; Lan, T.; Wang, X.; Rong, M.; Koratkar, N. Short period sinusoidal thermal modulation for quantitative identification of gas species. *Nanoscale* **2020**, *12*, 220−229.
(14) Yang, A.; Wang, D.; Wang, X.; Zhang, D.; Koratkar, N.; Rong, M. Recent advances in phosphorene as a sensing material. *Nano Today* **2018**, *20*, 13−32.
(15) Pan, Q.; Li, T.; Zhang, D. Ammonia gas sensing properties and density functional theory investigation of coral-like Au-SnSe2 Schottky junction. *Sens. Actuators, B* **2021**, *332*, 129440.
(16) Wu, P.; Yin, N.; Li, P.; Cheng, W.; Huang, M. The adsorption and diffusion behavior of noble metal adatoms (Pd, Pt, Cu, Ag and Au) on a MoS2 monolayer: a first-principles study. *Phys. Chem. Chem. Phys.* **2017**, *19*, 20713.
(17) Choi, S. Y.; Kim, Y.; Chung, H.-S.; Kim, A. R.; Kwon, J.-D.; Park, J.; Kim, Y.-L.; Kwon, S.-H.; Hahm, M. G.; Cho, B. Effect of Nb Doping on Chemical Sensing Performance of Two-Dimensional Layered MoSe2. *ACS Appl. Mater. Interfaces* **2017**, *9*, 3817−3823.
(18) Chen, D.; Zhang, X.; Tang, J.; Cui, Z.; Cui, H.; Pi, S. Theoretical study of monolayer PtSe2 as outstanding gas sensor to detect SF6 decompositions. *IEEE Electron Device Lett.* **2018**, *39*, 1405−1408.
(19) Gui, Y.; Cao, W.; Sun, Z.; Lv, G.; Tang, C. First-principle study on the structural and electronic properties of H2S and SO2 adsorption on Pd-doped MoS2 monolayer. *Mol. Phys.* **2020**, *118*, No. e1606462.
(20) Shaw, J. C.; Zhou, H.; Chen, Y.; Weiss, N. O.; Li, Y.; Huang, Y.; Duan, X. Chemical vapor deposition growth of monolayer MoSe2 nanosheets. *Nano Research* **2014**, *7*, 511−517.
(21) Gui, Y.; Shi, J.; Li, T.; Tang, C.; Xu, L. Platinum modified MoS2 monolayer for adsorption and gas sensing of SF6 decomposition products: A DFT study. *High Voltage* **2020**, *5*, 454.
(22) Zhang, G.; Wang, Z.; Zhang, X. Theoretical screening into Ru-doped MoS2 monolayer as a promising gas sensor upon SO2 and SOF2 in SF6 insulation devices. *Mol. Phys.* **2022**, *120*, No. e2018517.
(23) Wang, D.-W.; Wang, X.-H.; Yang, A.-J.; Chu, J.-F.; Lv, P.-L.; Liu, Y.; Rong, M. Z. MoTe2: A Promising Candidate for SF6

Decomposition Gas Sensors with High Sensitivity and Selectivity. *IEEE Electron Device Lett.* **2018**, *39*, 292.
(24) Zhu, H.; Cui, H.; He, D.; Cui, Z.; Wang, X. Rh-doped MoTe2 Monolayer as a Promising Candidate for Sensing and Scavenging SF6 Decomposed Species: a DFT Study. *Nanoscale Res. Lett.* **2020**, *15*, 129.
(25) Zhang, X.; Wang, J.; Chen, D.; Liu, L. The adsorption performance of harmful gas on Cu doped WS2: A First-principle study. *Mater. Today Commun.* **2021**, *28*, 102488.
(26) Chen, D.; Zhang, X.; Xiong, H.; Li, Y.; Tang, J.; Xiao, S.; Zhang, D. A First-Principles Study of the SF6 Decomposed Products Adsorbed Over Defective WS2 Monolayer as Promising Gas Sensing Device. *IEEE Trans. Device Mater. Reliab.* **2019**, *19*, 473−483.
(27) Xu, L.; Gui, Y.; Li, W.; Li, Q.; Chen, X. Gas-sensing properties of Ptn-doped WSe2 to SF6 decomposition products. *J. Ind. Eng. Chem.* **2021**, *97*, 452−459.
(28) Ma, Y.; Dai, Y.; Guo, M.; Niu, C.; Lu, J.; Huang, B. Electronic and magnetic properties of perfect, vacancy-doped, and nonmetal adsorbed MoSe2, MoTe2 and WS2 monolayers. *Phys. Chem. Chem. Phys.* **2011**, *13*, 15546.
(29) Zhang, Y.; Ye, H.; Yu, Z.; Liu, Y.; Li, Y. First-principles study of square phase MX2 and Janus MXY (M=Mo, W; X, Y=S, Se, Te) transition metal dichalcogenide monolayers under biaxial strain. *Phys. E* **2019**, *110*, 134−139.
(30) Cui, H.; Chen, D.; Zhang, Y.; Zhang, X. Dissolved gas analysis in transformer oil using Pd catalyst decorated MoSe2 monolayer: A first-principles theory. *Sustainable Mater. Technol.* **2019**, *20*, No. e00094.
(31) Cui, H.; Zhang, X.; Zhang, G.; Tang, J. Pd-doped MoS2 monolayer: A promising candidate for DGA in transformer oil based on DFT method. *Appl. Surf. Sci.* **2019**, *470*, 1035−1042.
(32) Cui, H.; Feng, Z.; Wang, W.; Peng, X.; Hu, J. J. I. S. J. Adsorption Behavior of Pd-Doped PtS_2 Monolayer Upon SF_6 Decomposed Species and the Effect of Applied Electric Field. *IEEE Sens. J.* **2022**, *22*, 6764−6771.
(33) Zhang, D.; Li, Q.; Li, P.; Pang, M.; Luo, Y. Fabrication of Pd-Decorated MoSe2 Nanoflowers and Density Functional Theory Simulation Toward Ammonia Sensing. *IEEE Electron Device Lett.* **2019**, *40*, 616−619.
(34) Cui, H.; Liu, Z.; Jia, P. Pd-doped C3N monolayer: A promising low-temperature and high-activity single-atom catalyst for CO oxidation. *Appl. Surf. Sci.* **2021**, *537*, 147881.
(35) Li, P.; Hong, Q.; Wu, T.; Cui, H. SOF2 sensing by Rh-doped PtS2 monolayer for early diagnosis of partial discharge in the SF6 insulation device. *Mol. Phys.* **2021**, *119*, No. e1919774.
(36) Cui, H.; Zhang, X.; Li, Y.; Chen, D.; Zhang, Y. First-principles insight into Ni-doped InN monolayer as a noxious gases scavenger. *Appl. Surf. Sci.* **2019**, *494*, 859−866.
(37) Tkatchenko, A.; DiStasio, R. A.; Head-Gordon, M.; Scheffler, M. Dispersion-corrected Møller-Plesset second-order perturbation theory. *J. Chem. Phys.* **2009**, *131*, 094106.
(38) Zhao, B.; Li, C. Y.; Liu, L. L.; Zhou, B.; Zhang, Q. K.; Chen, Z. Q.; Tang, Z. Adsorption of gas molecules on Cu impurities embedded monolayer MoS2 : A first-principles study. *Appl. Surf. Sci.* **2016**, *382*, 280−287.
(39) Cui, H.; Jia, P.; Peng, X.; Hu, X. Geometric, Electronic and Optical Properties of Pt-Doped C3N Monolayer Upon NOx Adsorption: A DFT Study. *IEEE Sens. J.* **2021**, *21*, 3602−3608.
(40) Aretouli, K. E.; Tsipas, P.; Tsoutsou, D.; Marquez-Velasco, J.; Xenogiannopoulou, E.; Giamini, S. A.; Vassalou, E.; Kelaidis, N.; Dimoulas, A. Two-dimensional semiconductor HfSe2 and MoSe2/HfSe2 van der Waals heterostructures by molecular beam epitaxy. *Appl. Phys. Lett.* **2015**, *106*, 143105.
(41) Wu, H.; Xia, Y.; Zhang, C.; Xie, S.; Wu, S.; Cui, H. Adsorptions of $C_5F_{10}O$ decomposed compounds on the Cu-decorated NiS_2 monolayer: a first-principles theory. *Molecular Physics* **2023**, No. e2163715.
(42) Lin, I. H.; Lu, Y. H.; Chen, H. T. Nitrogen-doped carbon nanotube as a potential metal-free catalyst for CO oxidation. *Phys. Chem. Chem. Phys.* **2016**, *18*, 12093−12100.
(43) Liang, X.-Y.; Ding, N.; Ng, S.-P.; Wu, C.-M. L. Adsorption of gas molecules on Ga-doped graphene and effect of applied electric field: A DFT study. *Appl. Surf. Sci.* **2017**, *411*, 11−17.
(44) Zhang, Y.; Yang, R.; Li, H.; Zeng, Z. Boosting Electrocatalytic Reduction of CO 2 to HCOOH on Ni Single Atom Anchored WTe 2 Monolayer. *Small* **2022**, *18*, 2203759.
(45) He, B.; Lv, P.; Wu, D.; Li, X.; Zhu, R.; Chu, K.; Ma, D.; Jia, Y. Confinement catalysis of a single atomic vacancy assisted by aliovalent ion doping enabled efficient NO electroreduction to NH 3. *J. Mater. Chem. A* **2022**, *10*, 18690.
(46) Pyykkö, P.; Atsumi, M. Molecular single-bond covalent radii for elements 1-118. *Chem.—Eur. J.* **2008**, *15*, 186−197.
(47) Wang, Y.; Wu, D.; Lv, P.; He, B.; Li, X.; Ma, D.; Jia, Y. Theoretical insights into the electroreduction of nitrate to ammonia on graphene-based single-atom catalysts. *Nanoscale* **2022**, *14*, 10862−10872.
(48) Murphy, L. R.; Meek, T. L.; Allred, A. L.; Allen, L. C. Evaluation and test of pauling's electronegativity scale. *J. Phys. Chem. A* **2000**, *104*, 5867−5871.
(49) Wang, Y.; Wang, M.; Lu, Z.; Ma, D.; Jia, Y. Enabling multifunctional electrocatalysts by modifying the basal plane of unifunctional 1T′-MoS2 with anchored transition metal single atoms. *Nanoscale* **2021**, *13*, 13390−13400.
(50) Huang, J.; Chu, J.; Wang, Z.; Zhang, J.; Yang, A.; Li, X.; Gao, C.; Huang, H.; Wang, X.; Cheng, Y.; Rong, M. Chemisorption of NO2 to MoS2 Nanostructures and its Effects for MoS2 Sensors. *ChemNanoMat* **2019**, *5*, 1123−1130.
(51) Wang, X. H.; Wang, A. J.; Yang, N.; Koratkar, J. F.; Chu, P. L.; Lv, M. Z. J. P. C. C. P.; Rong, M. Z. Effects of adatom and gas molecule adsorption on the physical properties of tellurene: a first principles investigation. *Phys. Chem. Chem. Phys.* **2018**, *20*, 4058−4066.
(52) Zhang, D.; Cao, Y.; Yang, Z.; Wu, J. Nanoheterostructure Construction and DFT Study of Ni-Doped In2O3 Nanocubes/WS2 Hexagon Nanosheets for Formaldehyde Sensing at Room Temperature. *ACS Appl. Mater. Interfaces* **2020**, *12*, 11979−11989.
(53) Li, S. S.*Semiconductor Physical Electronics*; Springer, 2006; Vol. *28*(3), pp 363−364.
(54) Zhang, D.; Xu, Z.; Yang, Z.; Song, X. High-performance flexible self-powered tin disulfide nanoflowers/reduced graphene oxide nanohybrid-based humidity sensor driven by triboelectric nanogenerator. *Nano Energy* **2020**, *67*, 104251.
(55) Zhang, D.; Wu, Z.; Zong, X.; Zhang, Y. Fabrication of polypyrrole/Zn2SnO4 nanofilm for ultra-highly sensitive ammonia sensing application. *Sens. Actuators, B* **2018**, *274*, 575−586.
(56) Zhang, Y.-H.; Chen, Y.-B.; Zhou, K.-G.; Liu, C.-H.; Zheng, J.; Zhang, H.-L.; Peng, Y. Improving gas sensing properties of graphene by introducing dopants and defects: a first-principles study. *Nanotechnology* **2009**, *20*, 185504.
(57) Vadalkar, S.; Chodvadiya, D.; Som, N. N.; Vyas, K. N.; Jha, P. K.; Chakraborty, B. An Ab-initio Study of the C18 nanocluster for Hazardous Gas Sensor Application. *ChemistrySelect* **2022**, *7*, No. e202103874.
(58) Jiang, Z.; Pan, Q.; Li, M.; Yan, T.; Fang, T. Density functional theory study on direct catalytic decomposition of ammonia on Pd (111) surface. *Appl. Surf. Sci.* **2014**, *292*, 494−499.
(59) Li, F.; Gao, X.; Wang, R.; Zhang, T.; Lu, G. J. S.; Chemical, A. B. Study on TiO2-SnO2 core-shell heterostructure nanofibers with different work function and its application in gas sensor. *Sens. Actuators, A* **2017**, *248*, 812−819.

https://doi.org/10.1021/acsomega.2c07456
ACS Omega 2023, 8, 4244−4250